Polym. Korea, Vol. 45, No. 2, pp. 286-293 (2021)
https://doi.org/10.7317/pk.2021.45.2.286

ISSN 0379-153X(Print)
ISSN 2234-8077(Online)

텅스텐이 도핑된 바나듐산화물 코어와 폴리이소프로필아크릴아마이드 쉘 구조를 보유한 열변색 하이브리드 나노입자

정상원 · 박상휘* · 유중환* · 박주현†

중앙대학교 지능형에너지산업학과, 화학신소재공학부, *KNW연구소

(2020년 11월 3일 접수, 2020년 12월 14일 수정, 2020년 12월 15일 채택)

Thermochromic Hybrid Nanoparticles Comprising a Tungsten-Doped Vanadium Dioxide Core and a Poly(*N*-isopropylacrylamide) Shell Structure

Sang Won Jung, Sang Hwi Park*, Jung Whan Yoo*, and Juhyun Park†

Department of Intelligent Energy and Industry, School of Chemical Engineering and Materials Science, Institute of Energy-Converting Soft Materials, Chung-Ang University, Seoul 06974, Korea

**KNW R&D Center, Donyu 2-ro 60, Paju-eup, Paju-city, Gyeonggi-do 10832, Korea*

(Received November 3, 2020; Revised December 14, 2020; Accepted December 15, 2020)

초록: 열변색 스마트 창호 소재로서 텅스텐이 도핑된 바나듐이산화물(W_xVO_2) 나노입자와 폴리이소프로필아크릴아미드(PNIPAm)의 하이브리드 나노입자가 실리카 쉘 형성 및 PNIPAm의 표면라디칼 중합반응에 의해 합성되었다. 하이브리드 나노입자의 수분산액은 섭씨 28도의 금속-절연체 전이온도를 보유한 W_xVO_2 코어와 섭씨 32도의 하한임계 용액온도를 보유한 PNIPAm 쉘의 특성으로 인해 가시광선에서 근적외선까지의 넓은 스펙트럼 범위에서 효과적인 열변색 특성을 보였다. 하이브리드 나노입자에서 PNIPAm의 함량을 고정시키고 W_xVO_2의 함량을 변화시키며 특성을 측정한 결과 섭씨 20도에서 40도의 온도 변화에서 25% 이상의 태양광 변조 변화를 구현하였으며 W_xVO_2의 함량증가에 따라 입자의 증가된 뭉침현상에 의해 투과도는 85%에서 15%까지 급격하게 감소하였다. 본 연구결과는 W_xVO_2와 PNIPAm의 하이브리드화가 효율적인 열변색 소재를 제조하기 위한 주요 기술이 될 수 있음을 보여준다.

Abstract: Hybrid nanoparticles based on tungsten-doped vanadium dioxide (W_xVO_2) nanoparticles and poly(*N*-isopropylacrylamide) (PNIPAm) for thermochromic smart window applications were synthesized via silica layer formation using (3-mercaptopropyl)trimethoxysilane (MPTMS) followed by the surface-mediated free radical polymerization of PNIPAm, resulting in the aqueous dispersion of the hybrid nanoparticles. The metal-insulator transition of the W_xVO_2 core at around 28 °C and the lower critical solution temperature of PNIPAm at around 32 °C enable the aqueous dispersion of the hybrid nanoparticles to present an efficient thermochromicity depending on the temperature over a broad spectral range from visible to near-infrared light. The difference in the solar modulation was over 25%, while the luminous transmittance (T_{lum}) significantly decreased from 85% to 15% with increasing W_xVO_2 composition in the hybrids. Our results suggest that the hybridization of W_xVO_2 and PNIPAm is a potential methodology for preparing efficient thermochromic materials.

Keywords: vanadium oxide, tungsten doping, poly(*N*-isopropylacrylamide), thermochromic, smart windows.

Introduction

Nowadays, technologies for saving energy are receiving widespread attention, with many materials and methods having been studied. Among them, thermochromic smart windows that can control the transmission of sunlight are popular energy-saving devices in buildings because energy consumption used for buildings accounts for 30-40% of the total energy consumption.[1,2] Energy can be saved by efficiently manipulating the amount of sunlight transmitted through the smart window.[3] For example, when the outside temperature is high, the smart window can reduce the amount of sunlight entering the building, thereby decreasing the cost of cooling the interior of the building. On the other hand, when the outside temperature is low, the smart window can transmit the sunlight, thus maximizing energy-saving efficiency through internal temperature control.[4]

†To whom correspondence should be addressed.
jpark@cau.ac.kr, ORCID 0000-0003-1300-5743

A representative thermochromic material used for smart windows is monoclinic vanadium dioxide (VO_2(M)). It presents a metal-insulator transition (MIT) at around 68 °C, above which its structure changes from monoclinic to tetragonal and is accompanied by a change in the electrical property of VO_2 from semiconducting to metallic.[5,6] The resulting reflection of near-infrared light (NIR) at a temperature above 68 °C enables smart windows utilizing VO_2 to present the highest solar modulation ability (T_{sol}) of 22.3% and an average luminous transmission ($T_{lum, average}$) of 42.8%.[7,8] However, the MIT temperature of pristine VO_2(M) is too high for practical smart window applications that require an MIT at around room temperature and also the thermochromic property is limited to the NIR range.[9,10] Thus, a new technology based on VO_2 with an MIT near room temperature and solar modulation capability in the visible-to-NIR range is strongly required.

A promising approach to resolve this issue is to combine tungsten-doped VO_2 (W_xVO_2) with a thermo-responsive polymer that can modulate sunlight transmission in the visible light range. When W^{6+} or Ti^{4+} is incorporated into the crystalline structure of VO_2, the donation of electrons and distortion of the crystalline structure results in a decrease in the MIT temperature of pristine VO_2(M) down to room temperature.[11-13] On the other hand, poly(*N*-isopropylacrylamide) (PNIPAm), an organic thermo-responsive polymer, has a lower critical solution temperature (LCST) at around 32 °C and has received wide attention in smart window applications due to their change of transparency from a transparent state to an opaque state when the temperature changes above the LCST.[14-19] Because of the aggregation and precipitation of polymer chains above the LCST, the aqueous solution of PNIPAm becomes cloudy, thereby blocking the transmission of visible light, which is useful for smart window applications. For example, a PNIPAm hydrogel film shows a high T_{lum} of 70.7% and ΔT_{sol} of 25.5% in the visible range.[17] Thus, one can expect that the hybridization of W_xVO_2 with PNIPAm will provide solar modulation capability in the visible-to-NIR range at around 30 °C, which should be useful for practical applications of smart windows. The hybridization of VO_2 and PNIPAm has already been reported.[7,14,17] However, those studies focused on microgel and film forms that are different from the aqueous solution systems in our study, and the hybridization of W_xVO_2 with PNIPAm has not yet been reported.

In this study, we demonstrate the fabrication and thermochromicity of hybrid nanoparticles comprising W_xVO_2 and PNIPAm prepared via the surface polymerization of PNIPAm

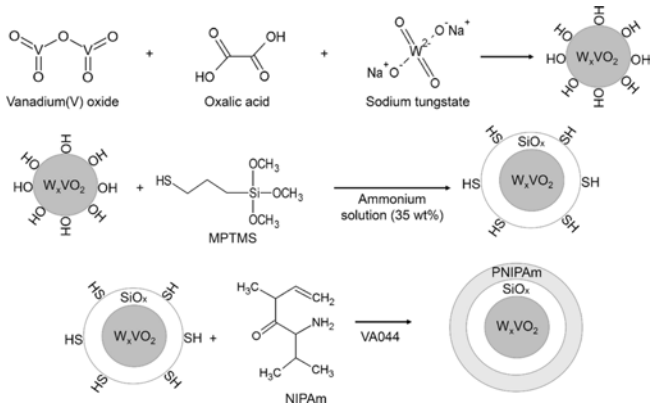

Scheme 1. Synthesis and coating procedure for W_xVO_2, W_xVO_2@MPTMS, and W_xVO_2@MPTMS@PNIPAm.

on W_xVO_2 nanoparticles in Scheme 1. Firstly, the W_xVO_2 nanoparticles was synthesized by hydrothermal synthesis with sodium tungstate. And then, a silica layer with surface thiol groups was first formed on the W_xVO_2 nanoparticles via the functionalization with (3-mercaptopropyl)trimethoxysilane (MPTMS) to provide surface thiol functionalities for polymerization and chemical stability[20] to the core W_xVO_2 under exposure to aqueous media. PNIPAm was then synthesized on the silica shell surface via free radical polymerization. The resulting hybrid organic-inorganic nanoparticles (W_xVO_2@MPTMS@PNIPAm) dispersed in an aqueous medium presented a reversible phase-transition property from a transparent (hydrophilic) to an opaque (hydrophobic) state at its LCST temperature, which is characteristic of PNIPAm.[14] Moreover, they presented an efficient solar modulation ability over the NIR range at around room temperature, which is characteristic of W_xVO_2. The aqueous dispersion of W_xVO_2@MPTMS@PNIPAm hybrid nanoparticles suggests the facile fabrication of smart windows by injecting the solution into an empty narrow space between two glass windows, which should be beneficial for simple, cost-effective fabrication.

Experimental

Materials. Oxalic acid dihydrate ($C_2H_2O_4{\cdot}2H_2O$), vanadium pentoxide (V_2O_5), sodium tungsten oxide dihydrate ($Na_2WO_4{\cdot}2H_2O$) were purchased from Alfa Aesar (Heysham, UK). *N*-isopropylacrylamide (NIPAm) and 2,2'-azobis[2-(2-imidazolin-2-yl)propane] dihydrate (VA044, $C_{12}H_{22}N_6{\cdot}2HCl$) were purchased from the Tokyo Chemical Industry (TCI, Tokyo, Japan). Polyvinylpyrrolidone (PVP, M_W~1300000 Da) and MPTMS ($SH(CH_2)_3Si(OCH_3)_3$) were purchased from Sigma-

Aldrich (St. Louis, MO, USA). All of the reagents were used as received.

W_xVO_2 Nanoparticles Synthesis. Oxalic acid (10.08 g, 0.112 mol) and V_2O_5 (7.27 g, 0.04 mol) were dissolved in deionized (DI) water (100 mL) in a three-neck round-bottomed flask equipped with a condenser for reflux. Na_2WO_4 (0.29 g; 2 mol% of W to V) was dissolved in 10 mL of DI water. The mixture was stirred at 400 rpm for 24 h at 60 °C. Afterward, the mixture was transferred to a Teflon-lined autoclave and the hydrothermal reaction was conducted at 185 °C for 12 h. After completing the reaction, the product was washed by centrifuging with ethanol three times and dried in a vacuum oven at room temperature for 24 h. The dried black-blue powder was calcinated at 700 °C for 2 h under a nitrogen atmosphere of a furnace.

W_xVO_2@MPTMS Coating. W_x-VO_2 (0.05 g) dispersed in ethanol (5 mL) via sonication for 30 min and PVP (0.128 g, 1.2 mmol on a repeat unit basis) dissolved in ethanol (10 mL) were added to a round-bottomed flask and stirred at room temperature for 72 h. Next, MPTMS solution (0.5 mL dissolved in 10 mL of ethanol) and ammonium solution (10 mL, 35 wt%) were added and stirred at room temperature for 12 h, resulting in a gray mixture solution. The precipitate was collected by centrifuging the solution at 8000 rpm for 15 min with excess ethanol to remove any uncoated W_xVO_2. The powder was dried in a vacuum at room temperature for 24 h.

W_xVO_2@MPTMS@PNIPAm Synthesis. In a three-neck round flask, W_xVO_2@MPTMS powder (0.05 g) was dispersed in DI water (10 mL) via sonication for 30 min, followed by the addition of VA044 (0.05 g, 0.155 mmol) in DI water (10 mL) and NIPAm (1.13 g; 10 mmol) in DI water (10 mL). The resulting solution was stirred at 60 °C for 4 h with nitrogen bubbling. Afterward, the solution mixture was precipitated in excess methanol (100 mL) to obtain a sticky solid product comprising black W_xVO_2 coated with white PNIPAm synthesized on the nanoparticle surfaces. This product was dried in a vacuum at room temperature for 24 h, which resulted in a hard product.

Characterization. Morphological observations of the nanoparticles shell were conducted by using a field-emission transmission electron microscope (FE-TEM; JEM-F200, JEOL, Japan). The crystalline structures of W_xVO_2(M) and VO_2(M) were verified via X-ray diffraction (XRD; Bruker-AXS NEW D8 Advance, Billerica, MA, USA). The MIT behaviors of W_XVO_2(M) and VO_2(M) were investigated using differential scanning calorimetry (DSC; Q-600, TA Instruments, Newcastle, DE, USA) analysis in the range of 20-130 °C at a heating rate of 10 °C/min. The thermochromic properties of W_xVO_2(M) and W_xVO_2@MPTMS@PNIPAm were measured with a UV-Vis-NIR spectrometer (V-770, JASCO, Tokyo, Japan) in the range of 300-2500 nm. Thermal decomposition behaviors were analyzed by thermogravimetric analysis (TGA; TA SDT Q600, TA Instruments, Newcastle, DE, USA) in the range of 20-600 °C at a heating rate of 10 °C/min.

Results and Discussion

The structures and phase-transition behavior of VO_2 and W_xVO_2 were analyzed via measurements from XRD patterns and DSC thermograms. The diffraction peaks in the observed XRD patterns of both VO_2 and W_xVO_2 were accurately matched with the monoclinic VO_2 crystalline structure (JCPDS NO.43-1051).[21] In the XRD patterns, sharp diffraction peaks for VO_2(M) at 26.8°, 27.8°, 33.4°, 37.0°, 39.8°, 42.1°, 42.2°, 55.5°, and 57.4°, corresponding to the (110), (011), (-102), (-202; -211; 200), (002), (-212;210), (-213; 220; 211), and (022) planes, show the high crystallinity of VO_2 and W_xVO_2 prepared in this study (Figure 1). The phase-transition behavior observed on the DSC thermograms clearly indicates the tungsten doping effect. When 2 mol% of tungsten to vanadium was added, the phase-transition temperature decreased from 66.9 to 27.9 °C, as shown in Figure 2(b). These results clearly show that although the small amount of tungsten incorporated into the pristine crystalline structure of VO_2 did not significantly modify the original structure, it did nevertheless decrease the

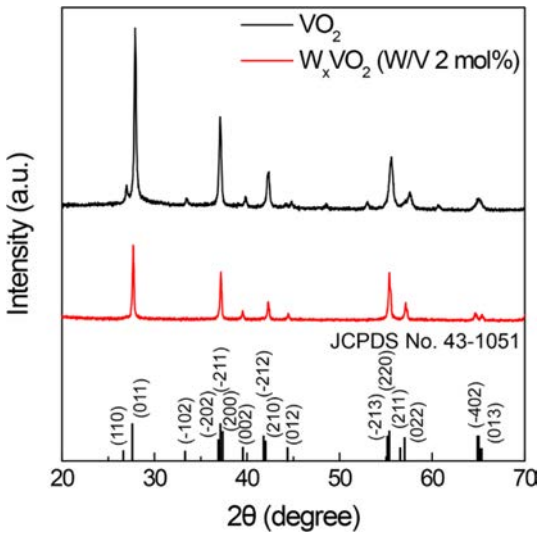

Figure 1. XRD patterns for VO_2 and W_xVO_2 (2 mol% W/V).

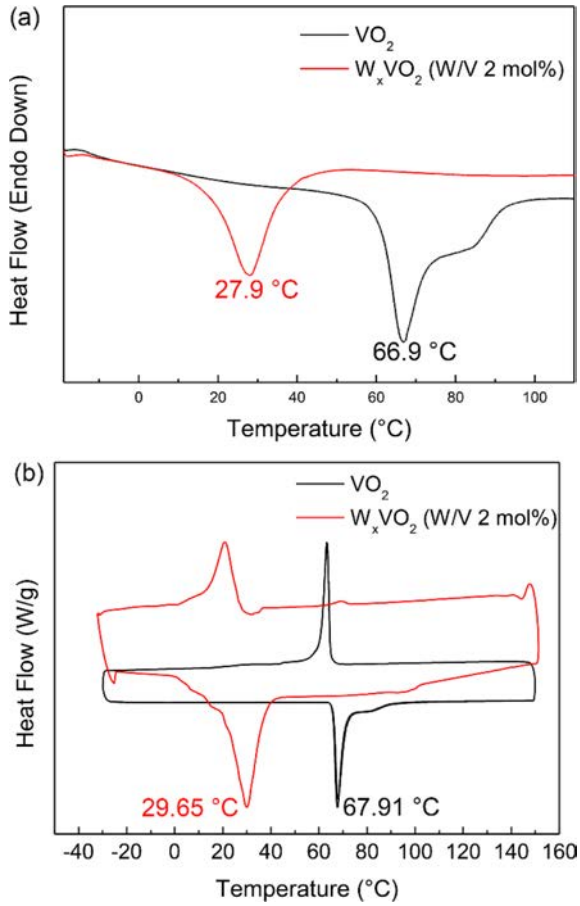

Figure 2. (a) DSC thermograms of VO_2 and W_xVO_2 (2 mol% W/V); (b) that at the third thermo-cycle.

MIT temperature to around room temperature. The shoulder peak appeared at around 80 °C in the DSC thermogram of VO_2 is ascribed to phase transition of agglomerate of particles. It should be noted that the shoulder peak is significantly weakened after multiple heating and cooling cycles as shown in Figure 2(b) and that the phase transition temperatures are slightly shifted to 29.7 and 67.9 °C for W_xVO_2 and VO_2, respectively. These results suggest that the agglomerates might be loosened and that the particles have stable phase transition behaviors over the multiple thermo-cycles.

To functionalize the surface of W_xVO_2 with thiol groups for the free radical polymerization of PNIPAm, W_xVO_2 nanoparticles were first coated with a silica layer. We used a literature procedure[21] except that we directly used MPTMS to form the silica shell with the thiol groups instead of using a conventional alkyl siloxane followed by MPTMS coating. In the process, PVP was first dissolved in ethanol and then mixed with an ethanol dispersion of W_xVO_2 nanoparticles, after which the

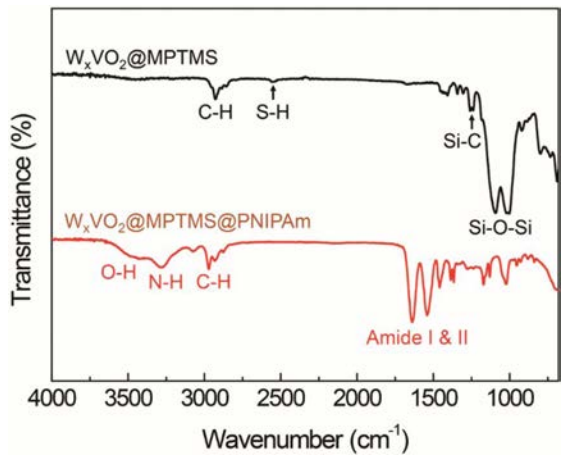

Figure 3. FTIR spectra of W_xVO_2 coated with a silica layer using MPTMS and with surface-polymerized PNIPAm (W_xVO_2@MPTMS@PNIPAm).

resulting mixture solution was stirred for 72 h to stabilize the nanoparticles via the adsorption of PVP chains on the nanoparticle surfaces.[22,23] Following this, the formation of the silica shell using MPTMS was carried out by adding it and an ammonium solution to hydrolyze and condense the siloxanes, which was followed by stirring for 12 h.[24-26] Gray nanoparticles were collected and the successful introduction of surface thiol groups was confirmed by measuring an FTIR spectrum and a TEM image of the nanoparticles. As shown in Figure 3, the FTIR spectrum of W_xVO_2 nanoparticles coated with a silica layer containing thiol groups show characteristic bands of C-H stretching of aliphatic alkyls (3000-2800 cm^{-1}), S-H stretching (2560.5 cm^{-1}), $-CH_2-$ bending (1407.8 cm^{-1}), Si-C bending (1258.8 cm^{-1}), and Si-O-Si asymmetric stretching (1092.5 & 1001.4 cm^{-1}).[27] The splitting of peaks at 1092.5 and 1001.4 cm^{-1} originates from the longitudinal and transverse optical vibrational modes of Si-O-Si asymmetric stretching vibration.[28] These very strong split peaks characteristic of Si-O-Si bonds suggest that the silica skeleton formed by hydrolysis and condensation of MPTMS on the surfaces of the W_xVO_2 nanoparticles was sufficiently ordered. Furthermore, the TEM image shown in Figure 4(a) clearly demonstrates the shell layer of the W_xVO_2 nanoparticle with a thickness of 40-50 nm, further confirming the successful synthesis of the silica shell. In addition, C-H and S-H stretching bands in the FTIR spectrum suggest the existence of thiol groups in the silica shell that are available for further surface reactions.

Preparation of hybrid nanoparticles of W_xVO_2 and PNIPAm was carried out by polymerizing PNIPAm on the surfaces of

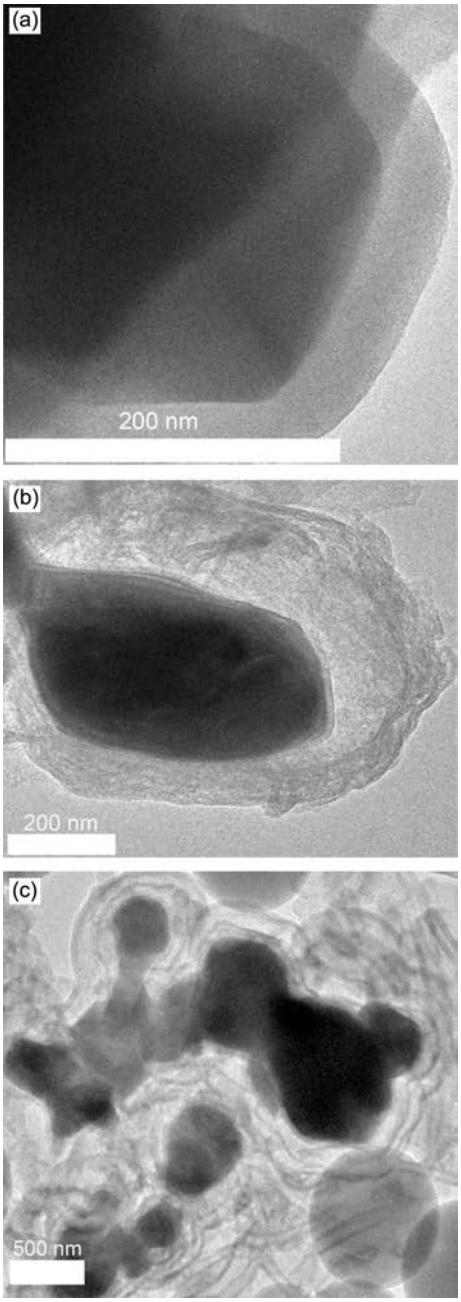

Figure 4. TEM images of (a) W_xVO_2@MPTMS; (b) W_xVO_2@MPTMS@PNIPAm at a high magnification; (c) at a low magnification.

the W_xVO_2 nanoparticles. NIPAm was polymerized via a free radical mechanism by utilizing a water-soluble azo-based radical initiator (VA044) and thiol groups as reacting sites on the surfaces of the W_xVO_2 nanoparticles.[29] The successful polymerization of PNIPAm on the surfaces of the W_xVO_2@MPTMS nanoparticles was confirmed via measurements on an FTIR spectrum (Figure 3) and a TEM image (Figure 4(b)). The

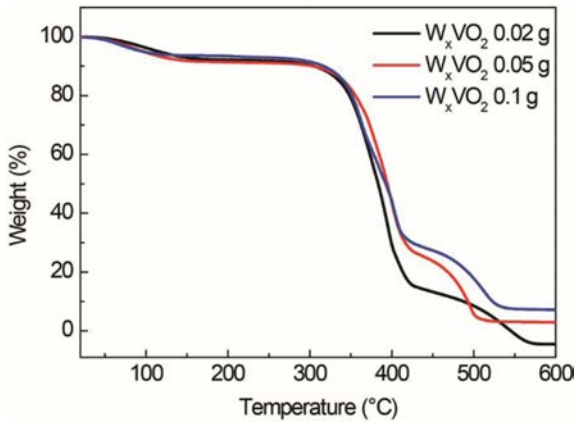

Figure 5. TGA pyrograms of W_xVO_2@MPTMS@PNIPAm with 0.02, 0.05, and 0.1 g of W_xVO_2.

FTIR spectrum of W_xVO_2@MPTMS@PNIPAm shows that the S-H peak at 2560.5 cm^{-1} disappears and that characteristic bands for PNIPAm,[30] including O-H stretching (~3433.2 cm^{-1}), NH stretching (3280.3 cm^{-1}), and C(=O)-N-H (1639.7 cm^{-1}, amide I; 1540.4 cm^{-1}, amide II), clearly appear. Moreover, PNIPAm on the W_xVO_2 nanoparticles was clearly observed as a light shell with a thickness of 100-200 nm surrounding the nanoparticles due to its low electron density in comparison to W_xVO_2, as shown in Figure 4(b) and 4(c). All of these results confirm that the hybrid structure of a W_xVO_2 core and a PNIPAm shell was successfully synthesized.

The compositions of these organic-inorganic hybrids were analyzed by measuring TGA pyrograms (Figure 5). Three distinct weight loss at around 100, 400 and 500 °C are allocated to the moisture evaporation, degradation of PNIPAm and inorganic components, respectively. We prepared three hybrid nanoparticles by using three different amounts of W_xVO_2(M) particles (0.02, 0.05, and 0.1 g) while the amount of NIPAm was fixed at 1.13 g, which means 1.7, 4.4, and 8.8 wt% of W_xVO_2 to PNIPAm in the hybrid nanoparticles. The residual weight percentages were -4.5, 2.9 and 7.2 wt%, respectively. Although the results show experimental errors, it was confirmed that W_xVO_2 nanoparticles were increasingly incorporated as designed.

The thermochromicity of the hybrid nanoparticles was examined in the wavelength range of 300-2500 nm using UV-Vis-spectroscopy below and above the phase-transition temperatures of W_xVO_2 and PNIPAm (20 and 40 °C, respectively). The hybrid nanoparticles were dispersed in DI water at 0.5 wt%; the resulting solutions are denoted as dispersions I, II, and III in the order of increasing W_xVO_2 weight percentage.

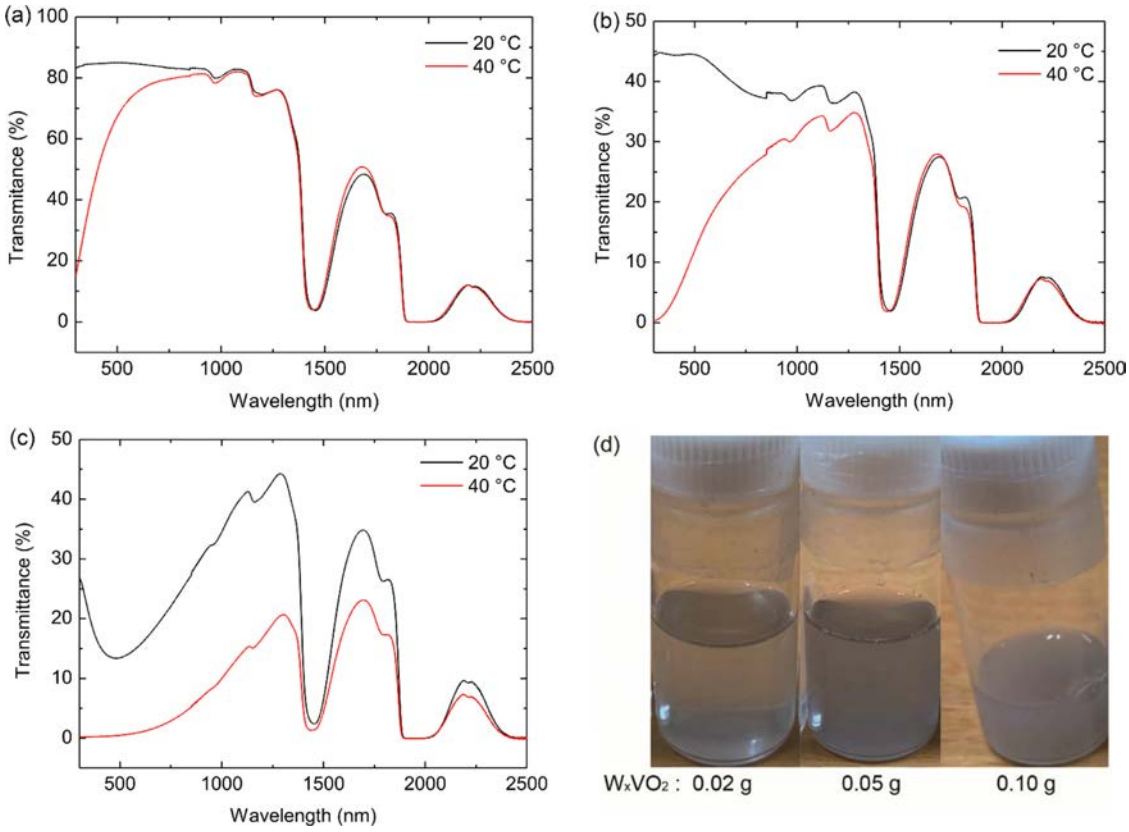

Figure 6. UV-Vis spectroscopy of W_xVO_2@MPTMS@PNIPAm with (a) 0.02 g of W_xVO_2; (b) 0.05 g of W_xVO_2; (c) 0.1 g of W_xVO_2; (d) optical images of W_xVO_2 dispersions in aqueous media.

The transmittance spectra of the three dispersion amounts measured at 20 and 40 °C were measured (Figure 6) and used to estimate their solar modulation (T_{sol}), solar modulation difference (ΔT_{sol}), and luminous transmittance (T_{lum}).

T_{sol} at each temperature was calculated as

$$T_{sol} = \frac{\int \varphi(\lambda) \cdot Tr(\lambda) \cdot d\lambda}{\int \varphi(\lambda) \cdot d\lambda} \quad (1)$$

where $\varphi(\lambda)$ and $Tr(\lambda)$ are the solar irradiation spectrum for an air mass of 1.5, corresponding to the sun standing 37° above the horizontal[31] and transmittance at specific wavelength λ, respectively.

ΔT_{sol} was estimated by applying[32]

$$\Delta T_{sol} = T_{sol}(20\ ^{o}C) - T_{sol}(40\ ^{o}C) \quad (2)$$

Finally, T_{lum} was calculated as

$$T_{lum} = \frac{\int \varphi_{lum}(\lambda) \cdot Tr(\lambda) \cdot d\lambda}{\int \varphi_{lum}(\lambda) \cdot d\lambda} \quad (3)$$

where $\varphi_{lum}(\lambda)$ is the spectral sensitivity of the light-adapted eye.[33]

The estimated ΔT_{sol} values utilizing the spectral variation depending on the temperature in Figure 5 were 5.4%, 13.9%, and 25.5% for the dispersions I, II, and III, respectively. These values show that the solar modulation ability of the hybrid nanoparticles was enhanced with increasing W_xVO_2 content. It is notable that the solar modulation of dispersion I with the lowest W_xVO_2 content can be mainly ascribed to spectral variations in the visible light range (Figure 6(a)) while the spectral variations in both the visible and NIR regions contribute to the enhanced ΔT_{sol} values of dispersions II and III (Figure 6(b) and 6(c)). Thus, it seems that W_xVO_2 at over 8 wt% in the hybrid nanoparticles with PNIPAm is necessary to observe a distinct contribution from the W_xVO_2 toward the thermochromicity over the visible-to-NIR range.

On the other hand, the T_{lum} values of dispersions I, II, and III at 20 °C decreased with increasing W_xVO_2 content (84.8, 42.4, and 14.7%, respectively). It should be mentioned that even though the ΔT_{sol} value of dispersion III is the highest, its T_{lum}

value of dispersion III is too low for practical applications. This can be ascribed to the size of hybrid nanoparticles being over a few hundred nanometers and their aggregation, which can severely scatter light and decrease light transmission. It should be mentioned that the polymerization of PNIPAm via the free radical mechanism can occur both in the medium and on the surfaces of W_xVO_2 nanoparticles. As a result, the particles can be even connected by PNIPAm chains as shown in the TEM image (Figure 4(c)). We presume that these agglomeration of the W_xVO_2 nanoparticles and PNIPAm chains cause such a severe light scattering in the NIR region and the nonlinear dependence of the NIR transmittance on the weight fraction of W_xVO_2 nanoparticles. However, our results suggest that the hybrid nanoparticles based on W_xVO_2 and PNIPAm with a particle size of less than 100 nm can present excellent thermochromicity in both the visible and NIR ranges.

Conclusions

In this study, we synthesized hybrid nanoparticles of tungsten-doped VO_2 core with a PNIPAm shell that had efficient thermochromicity for smart window applications over a broad spectral range (from the visible to the NIR region). Unlike conventional gel- or film-coating type thermochromic devices, our hybrid nanoparticles were designed to be applied as an aqueous dispersion that could simply be injected in between glass plates to simply achieve low-cost smart windows. W_xVO_2 nanoparticles were coated with a silica shell offering numerous thiol groups via the hydrolysis and condensation of MPTMS and finally, an outermost shell of PNIPAm synthesized via free radical polymerization utilizing the surface thiol groups. The resulting aqueous dispersions of the hybrid nanoparticles presented increasing ΔT_{sol} until the W_xVO_2 content reached 25%. However, it was noted that T_{lum} was drastically decreased down below 20% with the increase in W_xVO_2 in the hybrid nanoparticles, thereby making them unsuitable for practical applications. These issues suggest that further investigation should be carried out to determine the best route for synthesizing ultrafine tungsten-doped VO_2 with a diameter of less than 100 nm via a process that avoids aggregation. We believe that a novel synthetic route such as a modified polyol process[34] can provide W_xVO_2 nanoparticles with an MIT temperature at around RT and with a size less than 100 nm, enabling the formation of hybrids with negligible light scattering in the NIR region.

Acknowledgements: This research was supported by the Chung-Ang University Graduate Research Scholarship in 2019 and the Korea Institute of Energy Technology Evaluation and Planning, funded by the Ministry of Trade, Industry and Energy (Grant No. 20182020109500), Republic of Korea.

References

1. Kamalisarvestani, M.; Saidur, R.; Mekhilef, S.: Javadi, F. S. Performance, Materials and Coating Technologies of Thermochromic Thin Film on Smart Windws. *Renew. Sust. Energ. Rev.* **2013**, 26, 353-364.
2. Ke, Y.; Zhou, C.; Zhou, Y.; Wang, S.; Chan, S. H.; Long, Y. Emerging Thermal-Responsive Materials and Intergrated Thechniques Trageting the Energy-Efficient Smart Window Application. *Adv. Funct. Mater.* **2018**, 28, 1800113.
3. Kanu, S. S.; Binions, R. Thin Films for Solar Control Applications. *Proc. R. Soc. A* **2010**, 466, 19-44.
4. Cui, Y.; Ke, Y.; Liu, C.; Chen, Z.; Wang, N.; Zhang, L.; Zhou, Y.; Wang, S.; Gao, Y.; Long, Y. Thermochromic VO_2 for Energy-Efficient Smart Windows. *Cell Press, Joule, Rev.* **2018**, 2, 1707-1746.
5. Gao, Y.; Luo, H.; Zhang, Z.; Kang, L.; Chen, Z.; Du, J.; Kanehira, M.; Cao, C. Nanoceramic VO_2 Thermochromic Smart Glass: A Review on Progress in Solution Processing. *Nano energy* **2012**, 1, 221-246.
6. Morin, F. J. Oxides Which Show a Metal-to-insulatior Transition at the Neel Temperature. *Phys. Rev. Lett.* **1959**, 3, 34-36.
7. Wang, Y.; Zhao, F.; Wang, J.; Khan, A. R.; Shi, Y.; Chen, Z.; Zhang, K.; Li, L.; Gao, Y.; Guo, X. VO_2@SiO_2/Poly(N-isopropylacrylamide) Hybrid Nanothermochromic Microgels for Smart Window. *Ind. Eng. Chem. Res.* **2018**, 57, 12801-12808.
8. Chen, Z.; Gao, Y.; Kang, L.; Cao, C.; Chen, S.; Luo, H. Fine crystalline VO_2 Nanoparticles: Synthesis Abnormal Phase Transition Temperatures and Excellent Optical Properties of a Derived VO_2 Nanocomposite Foil. *J. Mater. Chem. A* **2014**, 2, 2718.
9. Wang, Y.; Zhao, F.; Wang, J.; Li, L.; Zhang, K.; Shi, Y.; Gao, Y.; Guo, X. Tungsten-Doped VO_2/Starch Derivative Hybrid Nanothermochromic Hydrogel for Smart Window. *Nanomaterials* **2019**, 9, 970.
10. Hu, L.; Tao, H.; Chen, G.; Pan, R.; Wan, M.; Xiong, D.; Zhao, X. Porous W-doped VO_2 Films with Simultaneously Enhanced Visible Transparency and Thermochromic Properties. *J. Sol-gel Technol.* **2016**, 77, 85-93.
11. He, Q.; Wang, Y.; Zhou, Y.; He, M.; Xu, R.; Hu, S.; Wu, W.; Wang, R. PAM-PNIPAM/W-doped VO_2 Thermochromic Hydrogel Film with High Solar Modulation Capability for Smart Windows Depolyment. *Opt. Mater.* **2019**, 97, 109367.
12. Liang, S.; Shi, Q.; Zhu, H.; Peng, B.; Huang, W. One-Step Hydrothernmal Synthesis of W-doped VO_2(M) Nanorods with a

Tunable Phase-Transition Temperature for Infrared Smart Windows. *ACS Omega* **2016**, 1, 1139-1148.
13. Houska, J.; Kolenaty, D.; Vlcek, J.; Barta, T.; Rezek, J.; Cerstvy, R. Significant Improvement of the Performance of ZrO_2/V1-xWxO_2/ZrO_2 Thermochromic Coatings by Utilizing a Second-order Interference. *Sol. Energy Mater. Sol. Cells* **2019**, 191, 365-371.
14. Wang, M.; Gao, Y.; Cao, C.; Chen, K.; Wen, Y.; Fang, D.; Li, L.; Guo, X. Binary Solvent Colloids of Thermosensitive Poly(N-isopropylacrylamide) Microgel for Smart Windows. *Ind. Eng. Chem. Res*. **2014**, 53, 18462-18472.
15. Seeboth, A.; Schneider, J.; Patzak, A. Materials for Intelligent Sun Protecting Glazing. *Sol. Energy Mater. Sol. Cells* **2000**, 60, 263-277.
16. Kim, D. J.; Kang, S. M.; Kong, B. K.; Kim, W. J.; Paik, H. J.; Choi, H. O.; Choi, I. S. Formation of Thermoresponsive Gold Nanoparticle/PNIPAAm Hybrids by Surface-Initiated, Atom Transfer Radical Polymerization in Aqueous Media. *Macromol. Chem. Phys.* **2005**, 206, 1941-1946.
17. Zhou, Y.; Cai, Y.; Hu, X.; Long, Y. VO_2/Hydrogel Hybrid Nanothermochromic Material with Ultra-high Solar Modulation and Luminous Transmission. *J. Mater. Chem.* **2015**, 3, 1121-1126.
18. Chen, T.; Zhang, S.; Hua, L.; Xu, Z.; Zhou, L.; Wang, J. Triphenylphosphine-Containing Thermo-Responsive Copolymers: Synthesis, Characterization and Catalysis Application. *Macromol. Res.* **2019**, 27, 931-937.
19. Xia, Y.; Wu, H.; Tang, D.; Gao, S.; Chen, B.; Zeng, Z.; Wang, S.; Cao, M.; Li, D. Graphene Oxide Nanosheet-Composited Poly(N-isopropylacrylamide) Hydrogel for Cell Sheet Recovery. *Macromol. Res*. **2019**, 27, 679-685.
20. Yang, S.-A.; Choi, S.; Jeon, S. M.; Yu, J. Silica Nanoparticle Stability in Biological Media Revisited. *Sci. Rep*. **2018**, 8, 186.
21. Jo, C. W.; Kim, H. J.; Yoo, J. W. Thermochromic Properties of W-Mo Co-Doped VO_2(M) Nanoparticles According to Reaction Parameters. *Nanosci. Nanotechnol.* **2017**, 17, 2923-2928.
22. Zou, H.; Schlaad, H. Thermoresponsive PNIPAM/Silica Nanoparticles by Direct Photopolymerization in Aqueous Media. *J. Polym. Sci., Part A: Polym. Chem.* **2015**, 53, 1260-1267.
23. Graf, C.; Vossen, D. L. J.; Imhof, A.; Blaaderen, A. V. A General Method To Coat Colloidal Particles with Silica. *Langmuir* **2003**, 19, 6693-6700.
24. Lee, J. C.; Choi, D. H.; Chou, J. Y.; Ha, C. S. Poly(lactic acid)/Functionalized Silica Hybrids by Reactive Extrusion: Thermal, Rheological, and Degradation Behavior. *Macromol. Res.* **2020**, 28, 327-335.
25. Ganguly, S.; Mondal, S.; Das, P.; Bhawal, P.; Das, T. K.; Ghosh, S.; Remanan, S.; Das, N. C. An Insight Into the Physico-Mechanical Signatures of Silylated Graphene Oxide in Poly(ethylene methyl acrylate) Copolymeric Thermoplastic Matrix. *Macromol. Res.* **2019**, 27, 268-281.
26. Xaiver, J. R. Experimental Investigation of the Hybrid Epoxy-Silane Coating for Enhanced Protection against the Corrosion of Aluminum Alloy AA7075 Frame in Solar Cells. *Macromol. Res.* **2020**, 28, 501-509.
27. Senkevich, J. J.; Mitchell, J.; Yang, G. R.; Lu, T. M. Surface Chemistry of Mercaptan and Growth of Pyridine Short-Chain Alkoxy Silane Molecular Layers. *Langmuir* **2002**, 18, 1587-1594.
28. Chem, W. H.; Tseng, Y. T.; Hsieh, S.; Liu, W. C.; Hsieh, C. W.; Wu, C. W.; Huang, C. H.; Lin, H. Y.; Chen, C. W.; Lin, P. Y.; Chau, L. K. Silanization of Solid Surfaces Viamercaptopropylsilatrane: A New Approach of Constructing Gold Colloid Monolayers. *RSC. Adv.* **2014**, 4, 46527-46535.
29. Abel, S. B.; Riberi, K.; Rivarola, C. R.; Molina, M.; Barbero, C. A. Synthesis of a Smart Conductive Block Copolymer Responsive to Heat and Near Infrared Light. *Polymers* **2019**, 11, 1744.
30. Zhu, D.; Lu, M.; Guo, J.; Liang, L.; Lan, Y. Effect of Adamantyl Methacrylate on the Thermal and Mechanical Properties of Thermosensitive Poly(N-isopropylacrylamide) Hydrogels. *J. Appl. Polym. Sci.* **2012**, 124, 155-163.
31. ASTM G173-03 Standard Tables of Reference Solar Spectral Irradiances: Direct Normal and Hemispherical on a 37 of Energy Technology Evaluation and Planning(ublic of Korea. studied for better in subsequen Materials, Philadelphia, PA, USA, http://rredc.nrel.gov/solar/spectra/am1.5.
32. Choi, Y. W.; Sim, D. M.; Hur, Y. H.; Han, H. J.; Jung, Y. S. Synthesis of Colloidal VO_2 Nanoparticles for Thermochromic Applications. *Sol. Energy Mater. Sol. Cells* **2018**, 176, 266-272.
33. Zhang, H.; Xiao, X.; Lu, X.; Chai, G.; Sun, Y.; Zhan, Y.; Xu, G. A Cost-effective Method to Fabricate VO_2 (M) Nanoparticles and Films with Excellent Thermochromic Properties. *Alloys. Compd* **2015**, 636, 106-112.
34. Lee, Y.; Jung, S. W.; Park, S. H.; Yoo, J. W.; Park, J. Synthesis of Tungsten-Doped Vanadium Dioxide Using a Modified Polyol Method Involving 1-Dodecanol. *Materials* **2020**, 13, 5384.